THE JOURNAL OF PHYSICAL CHEMISTRY C

Article

pubs.acs.org/JPCC

Electronic Excited State Specific IR Spectra for Phenylene Ethynylene Dendrimer Building Blocks

Johan F. Galindo,[†] Sebastian Fernandez-Alberti,[‡] and Adrian E. Roitberg*[,†]

[†]Department of Chemistry, Quantum Theory Project, University of Florida, Gainesville, Florida, 32611, United States

[‡]Universidad Nacional de Quilmes, Roque Saenz Peña 352, B1876BXD Bernal, Argentina

Supporting Information

ABSTRACT: Dendrimers are excellent candidates for applications in molecular devices and light harvesting where creating an energy gradient is crucial. Poly(phenylene ethynylene) (PPE) molecules are building blocks for dendrimers that also display the necessary characteristics for efficient energy transfer, including differential spatial localization associated with different excited states. In this work we calculated the ground state (S_0) as well as the excited IR spectra for the S_1 and S_2 states of ortho- and meta- substituted PPE (*o*-PPE and *m*-PPE). To compute IR spectra, a conformational space exploration was performed using ground-state classical molecular dynamics followed by direct adiabatic and non-adiabatic excited state molecular dynamics. IR spectra were computed from the autocorrelation function of the dipole moment in each state. We identified a band at 2150 cm^{-1} that is characteristic of S_1 in *m*-PPE. We show that in *m*-PPE, S_1 and S_2 have transition densities localized over different regions of the molecule, while in *o*-PPE the states are spread over the entire molecule. We find that the coupling between vibrations associated to the C≡C triple bonds plays an important role in the non-adiabatic electronic energy transfer. These results are a guide to the experimental characterization of the specific electronic excited states vibrations of these molecules.

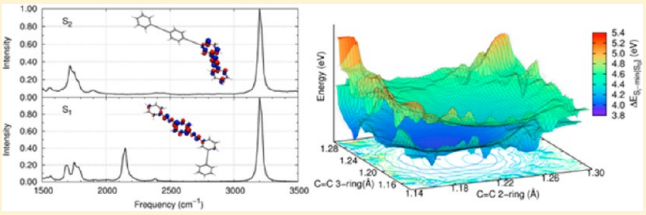

INTRODUCTION

The synthesis of new types of dendritic macromolecules opened new possibilities in molecular devices,[1,2] drug delivery,[3] and light harvesting.[4,5] Dendrimers are highly branched, monodisperse macromolecules[3] that can possess varied, well-defined three-dimensional structures. They are characterized by three basic elements: a single core; peripheral subunits known as branches (the number of branches grows geometrically with the number of generations); and finally the end groups. The synthesis of dendrimers has evolved to allow better control in their design,[6−8] particularly in the localization of the functional groups within the dendritic network. Thanks to this control in the synthesis researchers are able to design molecules with special photophysical, photochemical, electrochemical, or catalytic properties. In the particular case of energy transfer processes the success in the use of dendrimers is due to the use of peripheral chromophores that absorb the light and funnel it to a central core. This process is associated with the π-conjugation that chromophores confer to the dendrimer molecule.[9]

The Moore group has synthesized a molecule known as the nanostar, which represents a class of designer molecules featuring excellent photostability and a high quantum yield. These properties could make this supermolecule an excellent candidate for application as supertips in optical nanoprobes and nanosensors.[10,11] In the nanostar, para-substituted poly-phenylene ethynylene (PPE) units are used as branch groups decreasing in size as the number of generations increases. The length of these branches goes from a four-ring system, to a three-ring system and finally a two-ring system. This design creates an energy gradient that directs the energy from the antenna to the core of the molecule.[12−16] The linear PPE units described above are connected to each other and to the core through meta-positions. Meta-substitution breaks electronic conjugation and weakens the electronic coupling between the linear PPE units. As a consequence of the local disorder the excited states of the molecule are confined to the linear PPE chains for symmetric dendrimers.[9,17]

For unsymmetrical PPE dendrimers different than the nanostar, the ortho substitution has also been evaluated;[18] the introduction of this branching produces an asymmetry in the network without breaking the conjugation of the PPE units, but causes the termination of the tree structure due to steric hindrance.[9]

Smaller PPE fragments can already mimic the ultrafast and highly efficient energy transfer process that occurs in larger dendrimers like the nanostar.[19,20] The PPE fragments have also been shown to be important in the design of energy transfer devices;[9,20,21] therefore, a correct characterization of their excited states is vital for their improvement.

It has been observed that in substituted PPE molecules the introduction of side groups on the phenyl rings causes a small blue shift of the single absorption band.[22] However, the emission

Received: October 16, 2013
Revised: November 25, 2013
Published: November 26, 2013

   dx.doi.org/10.1021/jp4102652 | *J. Phys. Chem. C* 2013, 117, 26517−26528

spectrum in this group of molecules shows a split band in the 400−500 nm range. This split has been associated to vibronic coupling between the ring stretching modes and the electronic transition.[22,23]

The two PPE molecular systems studied in this work are shown in Figure 1. We will refer to them as meta-poly-

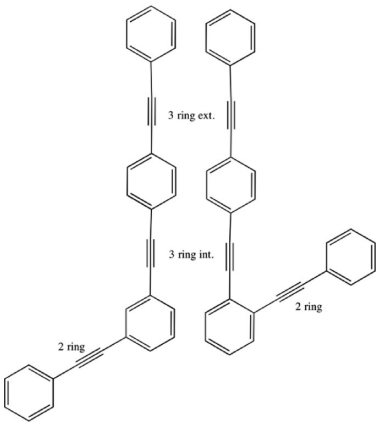

Figure 1. Molecules that involve two- and three- ring linear poly(phenylene ethynylene) units (*m*-PPE and *o*-PPE). Labels over the triple bonds have been done in order to distinguish them based on their position.

(phenylene-ethynylene) (*m*-PPE) and ortho-poly(phenylene-ethynylene) (*o*-PPE), based on the type of substitution in the benzene rings. Because of the different degree of conjugation of these two fragments, the excited states of these systems can display different spectroscopic properties.

The *m*-PPE fragments can be good candidates for the design of energy transfer molecules due to differential spatial localization in different excited states.[9] In contrast, *o*-PPE ones have shown a larger degree of delocalization of the excitation energy throughout the molecule, and they find applications in the design of energy transfer molecules as end groups.[9] *m*-PPE is able to transfer energy with a quantum yield close to 1 after a vertical excitation from the ground state (S_0) to the second excited state (S_2).[24] After this excitation, the energy gap between the first excited state (S_1) and S_2 decreases as the molecule evolves in the S_2 potential energy surface until it reaches a conical intersection between both states, where the electronic population is transferred to S_1. This process has been evaluated from a theoretical and experimental perspective.[19,24−28] The aim of the present work is to characterize electronic excited-state specific vibrations on *m*-PPE and *o*-PPE fragments to encourage new transient IR experimental studies focused on the intramolecular vibrational energy flow that takes place during the electronic excited-state relaxation. Although these type of experiments have not been performed on PPE yet, examples of excited state IR spectroscopy,[29−31] ultrafast time-resolved IR spectroscopy,[32−34] and ultrafast transient IR spectroscopy[35] are available in the literature. These techniques have been shown to be a powerful tool to study the decay of excited states.

THEORETICAL METHODOLOGY

Different approaches have been developed and used to compute electronic excited states.[36−41] One of the most efficient methodologies is the Collective Electronic Oscillator approach (CEO), which has been developed by Mukamel and co-workers.[40,42] In this work, we employ this approach combined with the Austin Model 1 (AM1)[43] to compute the electronic potential surface of the first two excited states of the system while using AM1 alone for the ground state dynamics. The agreement between AM1 and TDDFT at the B3LYP/6-31G(d,p) basis set has been shown to be good for the calculation of vertical excitation energies for the types of molecules studied in this manuscript.[24]

We will now describe the theoretical basis for the excited states calculation by using CEO,[40,42,44] Surface Hopping Dynamics,[45,46] IR spectroscopy,[47] and normal-mode analysis.[48,49]

Excited States Calculation. We can consider a system with n electrons that can occupy k molecular orbitals. The eigenstates of the molecular time independent Hamiltonian ($\hat{H}\psi_\alpha(R) = E_\alpha\psi_\alpha(R)$, where α is a particular excited state of the system) are obtained as a single Slater determinant $\psi_\alpha = |\phi_1(1)\text{-}\phi_2(2)...\phi_k(n)\rangle$, where $\phi_i(i)$ correspond to a molecular orbital that is a linear combination of atomic orbital basis functions. The molecular time independent Hamiltonian used in this work corresponds to the one associated with the AM1 semiempirical method, and the eigenstates obtained are also the ones associated with this method.

The reduced single electron density matrix for every state of the system can be written as:

$$(\boldsymbol{\rho}_{0\alpha})_{nm} \equiv \langle\psi_\alpha|c_m^\dagger c_n|\psi_0\rangle \tag{1}$$

where $c_m^\dagger$ and c_n are the Fermi creation and annihilation operators and n and m correspond to atomic orbitals. ψ_α is the αth excited state and ψ_0 is the ground state. Then, $\boldsymbol{\rho}_{00}$ corresponds to the ground state density matrix and $\boldsymbol{\rho}_{0\alpha} = \boldsymbol{\xi}_\alpha$ are transition density matrices, which represent the changes in the density matrix when the system changes from the ground state to an excited state, induced by an optical transition. The transition density matrices are eigenfunctions of the two-particle Liouville operator ($\hat{\mathcal{L}}$)

$$\hat{\mathcal{L}}\boldsymbol{\xi}_\alpha = \Omega_\alpha\boldsymbol{\xi}_\alpha \tag{2}$$

where the eigenvalue Ω_α is the difference in energy between the ground state and the excited state ($\Omega_\alpha = E_\alpha - E_0$). The transition density matrices meet the following normalization condition

$$\boldsymbol{\xi}_\alpha^\dagger\cdot\boldsymbol{\xi}_\beta = Tr(\boldsymbol{\rho}_{00}[\boldsymbol{\xi}_\alpha, \boldsymbol{\xi}_\beta]) = \delta_{\alpha\beta} \tag{3}$$

The transition density matrix can be represented as $\boldsymbol{\xi} = \begin{bmatrix}\mathbf{X}\\ \mathbf{Y}\end{bmatrix}$, where only hole-particle ($\mathbf{Y}$) and particle-hole ($\mathbf{X}$) components are computed; therefore, eq 2 can be reformed for the molecular orbitals basis set as

$$\begin{bmatrix}\mathbf{A} & \mathbf{B}\\ -\mathbf{B} & -\mathbf{A}\end{bmatrix}\begin{bmatrix}\mathbf{X}\\ \mathbf{Y}\end{bmatrix} = \vec{\Omega}\begin{bmatrix}\mathbf{X}\\ \mathbf{Y}\end{bmatrix} \tag{4}$$

which is known as the first order random phase approximation (RPA). Matrix $\mathbf{A}$ in eq 4 is equal to the configuration interaction singles matrix (CIS). Therefore, it is possible to find a full solution to this equation by neglecting the $\mathbf{B}$ term. This approach is known as the Tamm-Dancoff approximation ($\mathbf{AX} = \vec{\Omega}\mathbf{X}$).

Avoiding the complete diagonalization of the Liouville operator ($\hat{\mathcal{L}}$) is possible because the action of $\hat{\mathcal{L}}$ over a single electron transition matrix can be computed on the fly as

$$\hat{\mathcal{L}}\boldsymbol{\xi} = [\mathbf{F}^{(\vec{R})}(\boldsymbol{\rho}_{00}), \boldsymbol{\xi}] + [\mathbf{V}^{(\vec{R})}(\boldsymbol{\xi}), \boldsymbol{\rho}_{00}] \tag{5}$$

where $\mathbf{F}^{(\vec{R})}(\boldsymbol{\rho}_{00})$ is the Fock matrix that depends parametrically on the nuclei coordinates R

dx.doi.org/10.1021/jp4102652 | J. Phys. Chem. C 2013, 117, 26517−26528

$$\hat{F}_{ij}^{(\vec{R})}(\boldsymbol{\rho}) = \hat{t}_{ij}^{(\vec{R})} + \hat{V}_{ij}^{(\vec{R})}(\boldsymbol{\rho}) \tag{6}$$

where $\hat{t}_{ij}^{(\vec{R})}$ are the kinetic operator acting over one-electron and $\hat{V}_{ij}^{(\vec{R})}(\boldsymbol{\rho})$ is the Coulomb and interchange operators acting over a density matrix

$$\hat{V}_{ij}^{(\vec{R})}(\boldsymbol{\xi}) = \sum_{ml}^{k} \xi_{kl}\left((ij|ml) - \frac{1}{2}(im|jl)\right) \tag{7}$$

Due to the use of AM1, the number of two-electron integrals that need to be computed is reduced, making it possible to work with large molecular systems.

Adiabatic Molecular Dynamics Simulation. The potential electronic surfaces for the ground and excited states are well-defined in the context of the Born−Oppenheimer approximation, where the energy as well as the wave function depend on the nuclear coordinates. To propagate the molecule in these potential surfaces, the forces need to be calculated ($\vec{F}_\alpha(\vec{R}) = -\nabla\vec{E}_\alpha(\vec{R})$). In the case of the ground state, the analytical gradient is

$$\nabla\vec{E}_0 = \frac{1}{2}Tr[(\mathbf{t}^{(\vec{R})} + \mathbf{F}^{(\vec{R})})\boldsymbol{\rho}_{00}] \tag{8}$$

For the excited state case the analytical gradient involves two different terms

$$\nabla\vec{E}_\alpha = \nabla\vec{E}_0 + \nabla\vec{\Omega}_\alpha \tag{9}$$

due to the fact that the energy of the excited state is $E_\alpha = E_0 + \Omega_\alpha$.

The gradient for the transition energy is

$$\nabla\vec{\Omega} = Tr[\mathbf{F}^{(\vec{R})}\mathbf{p}_{\alpha\alpha}] + Tr[\mathbf{V}^{(\vec{R})}(\xi_\alpha^\dagger)\boldsymbol{\xi}_\alpha] \tag{10}$$

The $\mathbf{p}_{\alpha\alpha}$ matrix is related to the excited state density matrix according to $\boldsymbol{\rho}_{\alpha\alpha} = \mathbf{p}_{\alpha\alpha} + \boldsymbol{\rho}_{00}$ and it is composed of two matrices:[42]

$$\mathbf{p}_{\alpha\alpha} = \mathbf{T}_{\alpha\alpha} + \mathbf{Z}_{\alpha\alpha} \tag{11}$$

The $\mathbf{T}_{\alpha\alpha}$ matrix is computed as the following anticommutator

$$\mathbf{T}_{\alpha\alpha} = [[\boldsymbol{\xi}_\alpha^\dagger, \boldsymbol{\rho}_{00}], \boldsymbol{\xi}_\alpha] \equiv (\mathbf{I} - 2\boldsymbol{\rho}_{00})(\boldsymbol{\xi}_\alpha^\dagger\boldsymbol{\xi}_\alpha + \boldsymbol{\xi}_\alpha\boldsymbol{\xi}_\alpha^\dagger) \tag{12}$$

with $\mathbf{I}$ being a unitary matrix. The $\mathbf{Z}_{\alpha\alpha}$ matrix is found solving the following linear equation

$$\hat{\mathcal{L}}\mathbf{Z}_{\alpha\alpha} = -\left[\left([[\boldsymbol{\rho}_{00}, \boldsymbol{\xi}_\alpha^\dagger], \mathbf{V}(\boldsymbol{\xi}_\alpha)] + \mathbf{V}\left(\frac{1}{2}[[\boldsymbol{\xi}_\alpha^\dagger, \boldsymbol{\rho}_{00}], \boldsymbol{\xi}_\alpha]\right)\right), \boldsymbol{\rho}_{00}\right] \tag{13}$$

Non-Adiabatic Molecular Dynamics. For the non-adiabatic molecular dynamics we used the fewest switches in the surface-hopping method introduced by Tully.[42,45,46] This method allows jumping between potential electronic surfaces coming from different states and is governed by the coefficients of the electronic wave function, in contrast to adiabatic dynamics in the Born−Oppenheimer (BO) approximation, which do not allow the transition between electronic energy surfaces.

Within the time-dependent Schrödinger equation

$$i\hbar\frac{\partial|\Psi(t)\rangle}{\partial t} = \hat{H}|\Psi(t)\rangle \tag{14}$$

the time dependent wave function can be written as a linear combination of the time independent wave function, multiplied by a time dependent coefficient

$$|\Psi(t)\rangle = \sum_\alpha C_\alpha(t)|\Psi_\alpha\rangle \tag{15}$$

Substituting eq 15 into 14, we obtain

$$i\hbar\dot{C}_\alpha(t) = C_\alpha(t)E_\alpha - i\hbar\sum_\beta C_\beta(t)\langle\psi_\alpha|\frac{\partial\psi_\beta}{\partial t}\rangle \tag{16}$$

Within the BO approximation, the term $i\hbar\sum_\beta C_\beta(t)\langle\psi_\alpha|\frac{\partial\psi_\beta}{\partial t}\rangle$ is zero and there is no possibility for surface hopping. The rightmost term, responsible for the non-adiabatic coupling between surfaces, can be modified using the chain rule, assuming that the atomic movement can be described by a trajectory $\vec{R}(t)$

$$\langle\psi_\alpha|\frac{\partial\psi_\beta}{\partial t}\rangle = \dot{\vec{R}}\cdot\langle\psi_\alpha(\vec{R})|\nabla_{\vec{R}}\psi_\beta(\vec{R})\rangle = \dot{\vec{R}}\cdot d_{\alpha\beta} \tag{17}$$

The non-adiabatic coupling vector between excited states ($d_{\alpha\beta}$) can be calculated analytically within the CEO framework using the Hellmann−Feynman theorem

$$\langle\psi_\alpha(\vec{R})|\nabla_{\vec{R}}\psi_\beta(\vec{R})\rangle = d_{\alpha\beta} = \frac{Tr[\mathbf{F}^{(\vec{R})}\boldsymbol{\rho}_{\alpha\beta}]}{\Omega_\alpha - \Omega_\beta} \tag{18}$$

Finally, the probability of a transition between a state α and another excited state β is calculated at each integration step of the trajectory as

$$g_{\alpha\to\beta} = -\frac{\Delta t}{\hbar}\frac{2\mathrm{Re}(C_\alpha(t)C_\beta^*(t)\dot{\vec{R}}\cdot d_{\alpha\beta})}{|C_\alpha(t)|^2} \tag{19}$$

with the condition that if $g_{\alpha\to\beta} < 0$ then $g_{\alpha\to\beta} = 0$. To determine whether a transition will take place or not, a random number $0 < \eta < 1$ is generated. The hop from the surface for the state α to state β will be performed if $0 < \eta < g_{\alpha\to\beta}$, and if $\sum_{\beta\neq\alpha} g_{\alpha\to\beta} < \eta < 1$ the system will remain in state α.

In both non-adiabatic and adiabatic dynamics, the evolution of the nuclear degrees of freedom in the excited potential surface is evaluated using the Langevin thermostat of motion

$$M_i\ddot{\vec{R}}(t) = -\nabla_R\vec{E}_\alpha(\vec{R}(t)) - \gamma M_i\dot{R}_i(t) + \zeta(t) \tag{20}$$

where $\zeta(t)$ is a random force[50] taken from a Gaussian distribution with a variance of $2M_ik_BT\gamma(\delta t)^{-1}$, γ is the friction coefficient, M_i is the mass of the ith nuclei, and $\ddot{R}_i(t)$ and $\dot{R}_i(t)$ are the acceleration and velocity, respectively. The introduction of this thermostat will help us mimic the effect of solvent friction that is present in experimental conditions.

IR Spectrum. In the case of IR spectroscopy, the matter−radiation interaction can be approximated by a dielectric dipole interaction. This approximation is valid when the molecular dimensions are small in comparison to the wavelengths of absorbed light.[47] It has been shown that the light−matter interaction Hamiltonian $\hat{H}_i(t)$ can be written as a free plane wave containing the phase terms $e^{i\omega t}$ and $e^{-i\omega t}$,[47] multiplied by the time-independent Hamiltonian $\hat{H}_i$. In the particular case of IR, $\hat{H}_i = \vec{\varepsilon}_0\hat{\mu}$ where $\hat{\mu}$ is the electric dipole moment operator and $\vec{\varepsilon}_0$ is the amplitude of the electric field. Using linear response theory, the IR line shape can be written as the Fourier Transformation of the dipole moment autocorrelation function ($\langle\mu(0)\mu(t)\rangle$)[51,52]

$$I(\omega) = \frac{D}{2\pi}\int_{-\infty}^{\infty}\langle\mu(0)\mu(t)\rangle_0 e^{-i\omega t}\,dt \tag{21}$$

dx.doi.org/10.1021/jp4102652 | J. Phys. Chem. C 2013, 117, 26517−26528

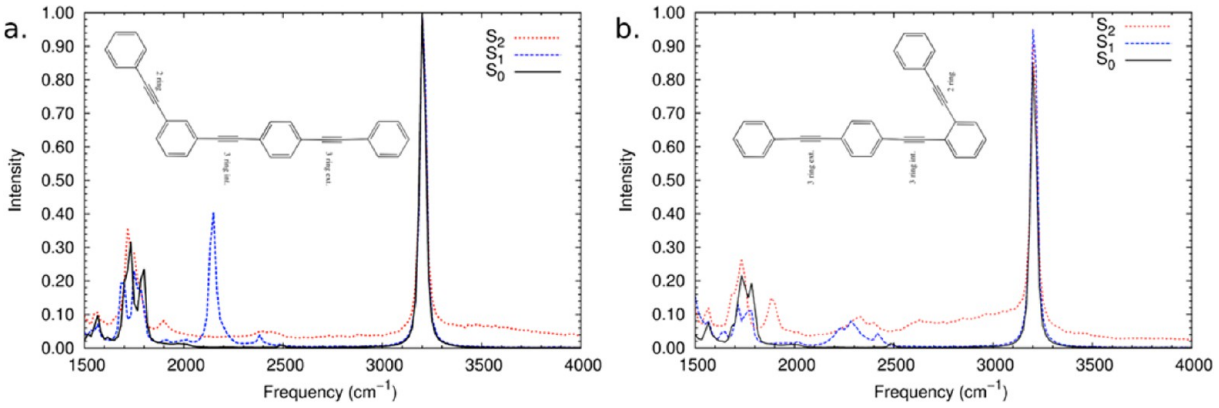

Figure 2. IR spectra for *m*-PPE (a) and *o*-PPE (b) substitution linkages. Three different spectra are shown: the ground state (S_0) and the first two excited states S_1 and S_2, respectively, for both substitutions.

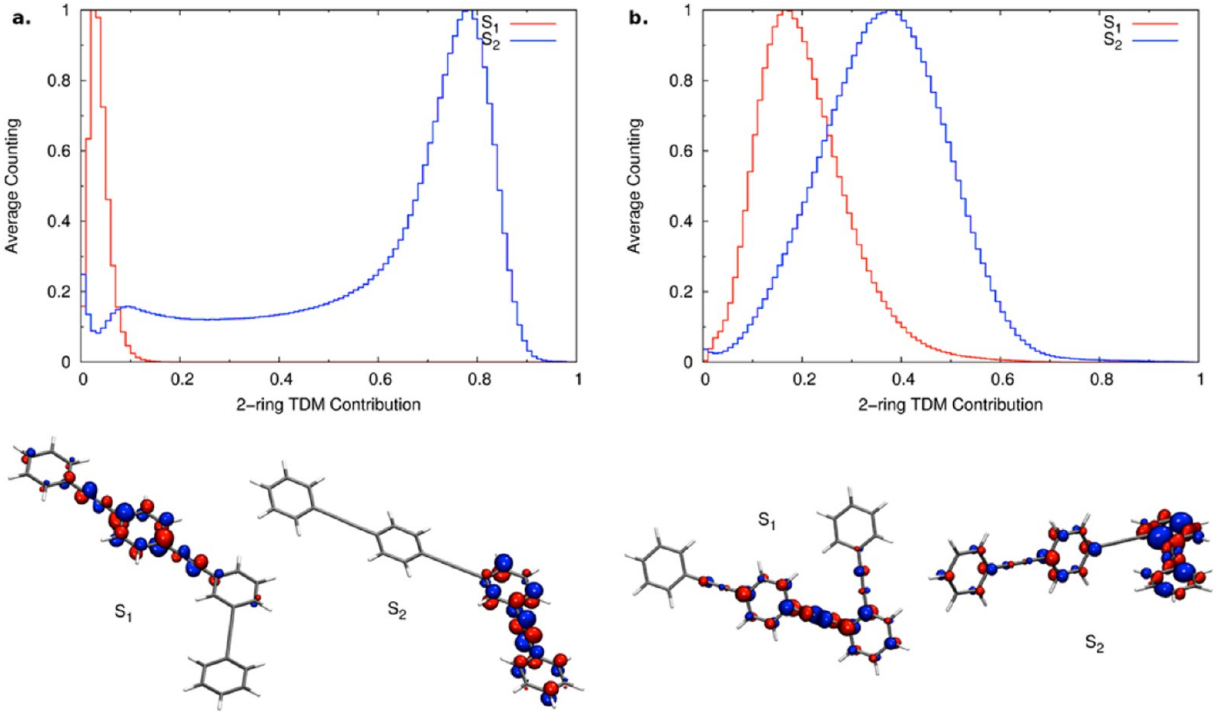

Figure 3. Histogram for the transition density matrix (TDM) over the 1000 different excited simulations. In the case of *m*-PPE (a) the main contribution for the S_1 excited state is located in the three-ring region, while for the S_2 state it is located in the two-ring part. For the case of *o*-PPE it is possible to observe that the S_2 state is delocalized in both segments, i.e., 2- and three-ring systems, while the S_1 state presents a higher contribution of the three-ring system (b). The bottom figures correspond to the transition densities at the minimum energy structure for both excited state surfaces, showing the localization of it for both systems, *m*-PPE and *o*-PPE.

where a quantum correction factor D needs to be included to account for detailed balance. There is a certain degree of arbitrariness in the choice of the quantum factor; however, the form[53,54]

$$D = \frac{\beta\hbar\omega}{1 - e^{-\beta\hbar\omega}} \tag{22}$$

has been shown to give the most accurate results on calculated IR amplitudes.

$$I(\omega) = \frac{\beta\hbar\omega}{2\pi(1 - e^{-\beta\hbar\omega})} \int_{-\infty}^{\infty} \langle \mu(0)\mu(t)\rangle_0 e^{-i\omega t}\, dt \tag{23}$$

To compute the IR spectrum using ESMD simulations, the dipole moment is calculated throughout the trajectories as:[55]

$$\vec{\mu}_\alpha = Tr[\boldsymbol{\mu}\boldsymbol{\rho}_{\alpha\alpha}] \tag{24}$$

Normal Mode Analysis. If IR spectra are different for different electronic excited states, then it can only mean that the curvature of the potential energies differs. It is common to express the excited state normal modes using the ground state modes as a reference. Excited-state vibrational normal modes ($\mathcal{Z}$) can be related to ground state vibrational modes by using the Duschinsky relation $\mathcal{Z}^\alpha = \mathbf{J}^{\alpha 0}\mathcal{Z}^0 + \mathbf{D}^{\alpha 0}$, where $\mathbf{J}$ is the Duschinsky rotational matrix and $\mathbf{D}$ is the equilibrium displacement between the ground state and the chosen excited state.[56] In the present work, we have neglected Duschinsky rotations, and the analysis of excited-state IR spectra has been performed on the basis of ground-state (S_0) modes ($\mathbf{J} = 1$).[49] In order to obtain

dx.doi.org/10.1021/jp4102652 | J. Phys. Chem. C 2013, 117, 26517−26528

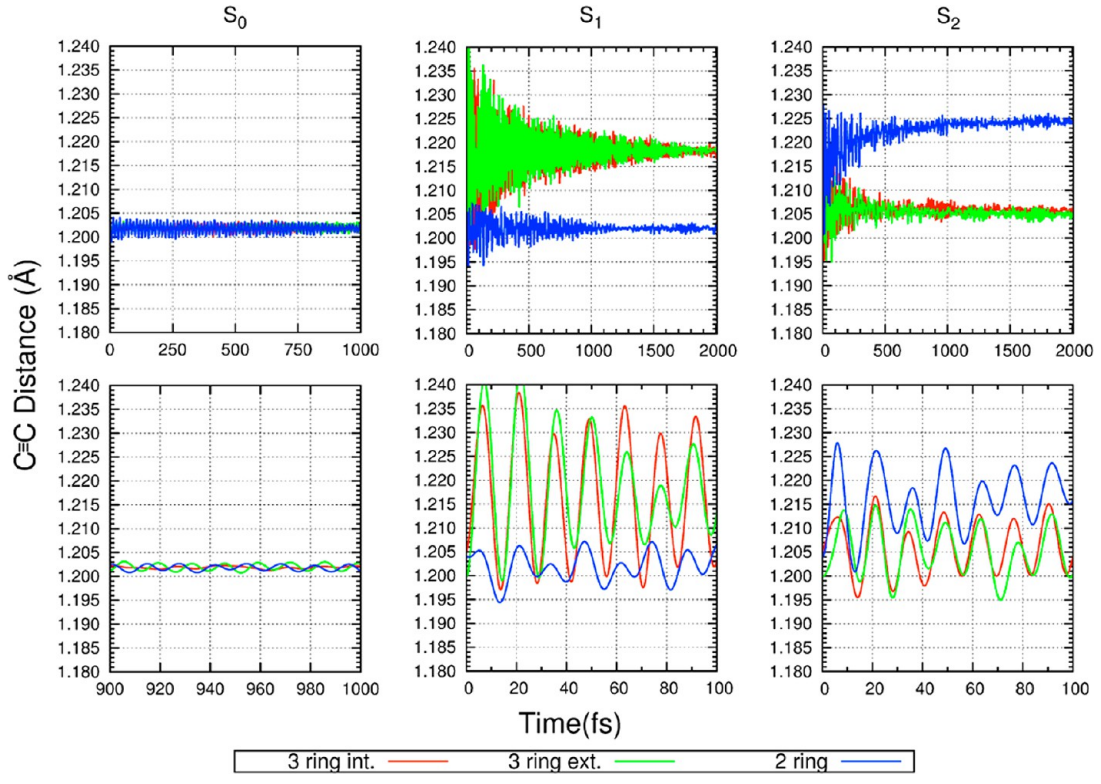

Figure 4. Triple bond distances as a function of time for *m*-PPE. The distances are presented for the ground state as well as the first two excited states. The bottom plots shows the last 100 fs for S_0 and the first 100 fs for S_1 and S_2 dynamics. The definition of the triple bonds (external and internal) is presented in Figure 1.

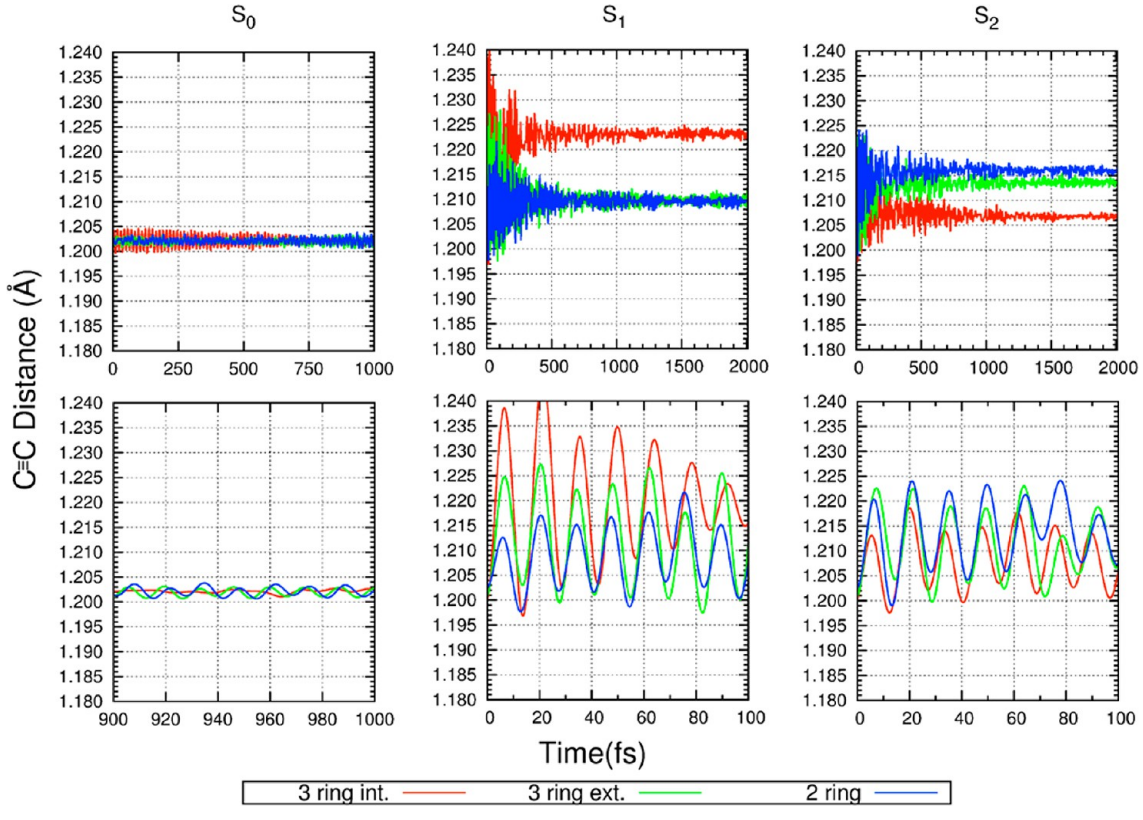

Figure 5. Triple bond distances as a function of time for *o*-PPE. The distances are presented for the ground state as well as the first two excited states. The bottom plots shows the last 100 fs for S_0 and the first 100 fs for S_1 and S_2 dynamics. The definition of the triple bonds (external and internal) is presented in Figure 1.

dx.doi.org/10.1021/jp4102652 | J. Phys. Chem. C 2013, 117, 26517−26528

these modes, we diagonalized the mass-weighted Hessian matrix $\mathbf{K}^0$ of the ground state at its minimum $\mathbf{R}_0^0$. That is,

$$\mathbf{L}^{\dagger}\mathbf{K}\mathbf{L} = \vec{\lambda}\,\mathbf{I} \tag{25}$$

The eigenvector matrix $\mathbf{L}$ can be used to relate the ground state normal modes to the relative displacements $q_i^{\alpha}(t)$ of the mass-weighted Cartesian *body fixed* coordinates in the α excited state according to $\{q_i^{\alpha}(t) = M_i^{1/2}\,(R_i^{\alpha}(t) - R_i^0)\}_{i=1,3n}$.

The normal modes displacements in terms of $q_i(t)$is obtained as

$$Q_j^{\alpha}(t) = \sum_{3n}^{i=1} l_{ij} q_i^{\alpha}(t) \tag{26}$$

where l_{ij} are the elements of $\vec{L}_j$ normal mode vector in the ground state.[48]

Computational Details. The *m*-PPE and *o*-PPE geometries were optimized at the AM1 semiempirical level using *Gaussian09*[57] and the final structures were employed as our initial guess in a molecular dynamics simulation. The parameters for the classical MD simulation of these molecules such as charges, angles, and dihedrals were taken from the GAFF force field,[58] and an additional rotational barrier of 0.20 kcal/mol over the angle between the planes containing the rings was included in order to reproduce the experimental torsional barrier.[13] The simulations were performed using the Langevin equation at constant temperature with a friction coefficient γ of 2.0 ps^{-1}.

The system was initially allowed to equilibrate during 10 ps arriving at a final temperature of 300 K using AMBER 12 program suite.[59] After this process, 50 ns of classical molecular dynamics at 300 K with a time step of 0.5 fs was used to collect a set of initial coordinates and momenta for the subsequent excited state molecular dynamics (ESMD) simulations.[42] These snapshots were taken every 50 ps, which means a final set of 1000 different structures was produced.

Each of the stored configurations sampled with the classical potential was subsequently relaxed for 1 ps in the ground state using a regular AM1 Hamiltonian, as implemented in our ESMD implementation.[42] Subsequently, an AM1 production of 2 ps with a time-step of 0.1 fs was performed for every snapshot at the ground state level in order to compute the ground state IR spectrum. The final configuration of the S_0 simulations after 2 ps was used to start two sets of 1000 nonequilibrium ESMD simulations: one where the each snapshot system is vertically excited from S_0 to S_1, and another one where it is excited to S_2. Each of these simulations was run for 2 ps at a constant temperature of 300 K and using an integration time for Newton's equations of 0.1 fs. The dipole moment was computed at every time-step of the dynamics for ground state and the excited states to compute the IR spectra.

RESULTS AND DISCUSSION

Infrared spectra for the ground state (S_0) and the first (S_1) and second (S_2) excited states were computed for both *m*-PPE and *o*-PPE as an average of 1000 different spectra (Figure 2). A blueshift for the benzene C−H stretching vibrations (3067−2900 cm^{-1}) is seen when comparing the calculated S_0 IR spectrum with the experimental one.[60] The same effect is observed in the case of the calculated C≡C acetylene stretching peak (2500 cm^{-1}), which is also blue-shifted with respect to the experimental value (2210 cm^{-1}).[60] Both the experimental and calculated bands have extremely low intensities, which barely register as IR active bands. Comparing the theoretical spectra of

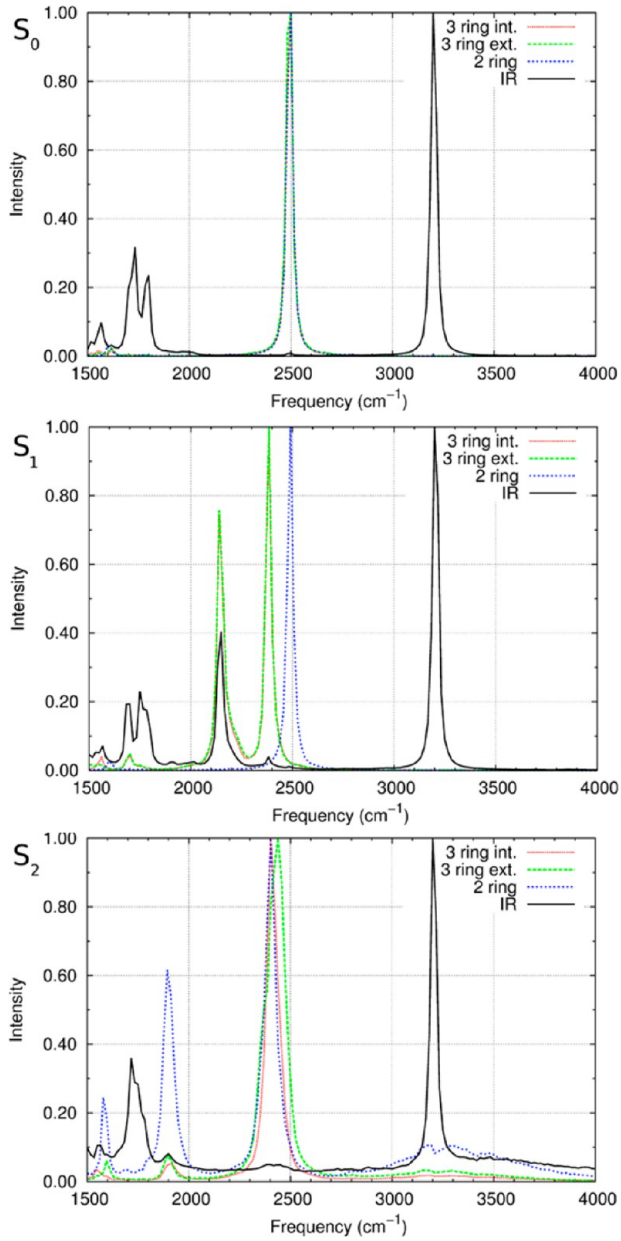

Figure 6. Distance spectra for the triple bond compared to the IR spectra for the ground state and the first two excited states of *m*-PPE.

the ortho and meta substituted molecules, we find no evidence that the substitution affects these two bands, which is in agreement with the IR experimental results for similar molecules.[60] The discrepancy between the experimental and theoretical spectra can be attributed to the use of the AM1 semiempirical method, and some authors have accounted for it by including correction factors.[61]

Comparison of the S_0, S_1, and S_2 spectra of the *m*-PPE molecule reveals the presence of state-specific vibrations that can be used as fingerprints to characterize each state. We can identify a specific S_1 state vibration in the region of 2150 cm^{-1}, that corresponds to a C≡C acetylene stretching band, which is red-shifted by 350 cm^{-1} compared to the same C≡C low intensity band for S_0 and S_2. This band is IR active in S_1, but not in the other two states. There are no other major noticeable differences for the spectra in the three states. Hence, these results allow us to suggest that it is possible to identify the S_1 state using IR

dx.doi.org/10.1021/jp4102652 | J. Phys. Chem. C 2013, 117, 26517−26528

Table 1. Participation Numbers of Every Triple Bond for Both Isomers[a]

	two-ring			three-ring int.			three-ring ext.			Molecule
$\mathcal{P}$		1.57			2.77			2.08		*m*-PPE
Mode	124	125	126	124	125	126	124	125	126	
$(\vec{V}\vec{L}_j)^2$	0.010	0.172	0.780	0.337	0.474	0.151	0.616	0.316	0.030	
$\mathcal{P}$		2.98			2.21			2.28		*o*-PPE
Mode	124	125	126	124	125	126	124	125	126	
$(\vec{V}\vec{L}_j)^2$	0.309	0.442	0.211	0.621	0.104	0.237	0.032	0.416	0.514	

[a]The normal mode number as well as its contribution is also presented. The underlined numbers correspond to the normal value with higher triple bond participation.

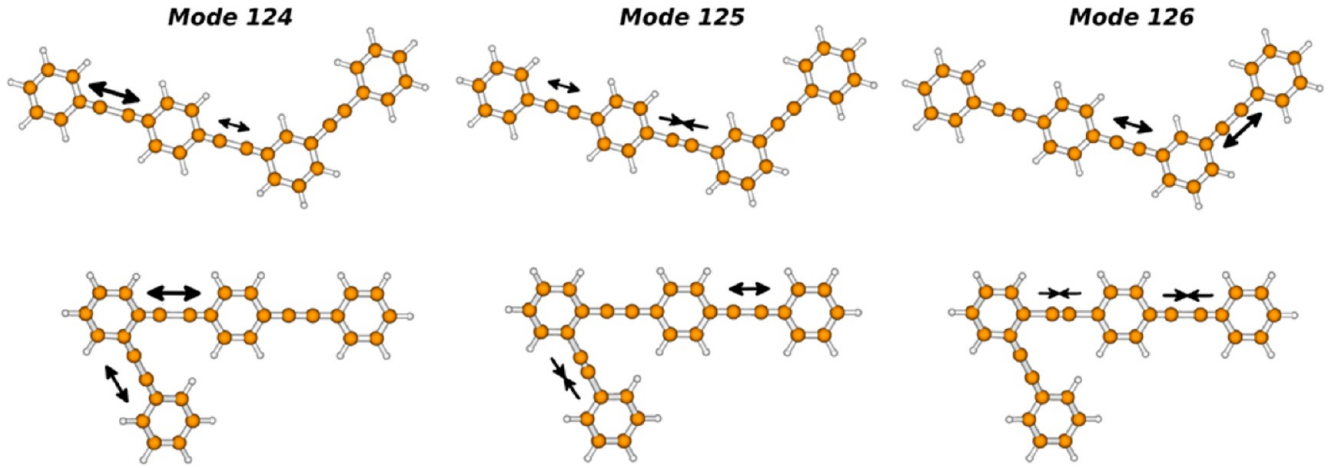

Figure 7. Normal modes where the triple bond atoms are more active for *m*-PPE and *o*-PPE in the S_0.

spectroscopy, since the presence of this characteristic peak is very notorious.

For *o*-PPE, the peaks around 2250 cm^{-1} are observed in both the S_1 and S_2 states, but it is less intense and broader compared to *m*-PPE. In the S_2 state, it is possible to characterize the molecule by a unique vibration around 1900 cm^{-1}. By comparison of both molecules, it is possible to ensure that IR spectroscopy allows the distinction between the excited states in both cases.

In order to better characterize state-specific vibrations, a detailed analysis of the ESMD simulations was performed. For this purpose, results concerning the spatial localization of the electronic transition densities, bond-distance distributions, and normal modes analysis were obtained for the different electronic states.

In the CEO approach, changes in the distribution of the electronic density induced by photoexcitation from ground state 0 to an excited electronic α state are followed through the diagonal elements of $(\rho_{0\alpha})_{nm}$[17] with the required normalization condition $\sum_{n,m}(\rho_{0\alpha})^2_{nm} = 1$, according to the CIS approximation.[62] Therefore, the fraction of the transition density localized on the different moieties of the *m*-PPE and *o*-PPE molecules can be calculated as

$$(\rho_{0\alpha})^2_X = \sum_{n_A,m_A}(\rho_{0\alpha})^2_{n_Am_A} + \frac{1}{2}\sum_{n_B,m_B}(\rho_{0\alpha})^2_{n_Bm_B} \quad (27)$$

where index A runs over all atoms localized in the *X*-moiety (*X* = two-ring, three-ring linear PPE units), and index B runs over atoms shared between these units.

Figure 3 depicts the extent of delocalization of the electronic transition density for each state, in each molecule. It is depicted as a histogram over all the 1000 ESMD. Since the transition density is normalized, we can state that if the transition density is not, for instance, localized in the two-ring system, then it must be localized in the three-ring system of the molecule. The electronic transition densities of the different electronic excited states of *m*-PPE are well localized on the individual moieties. While the S_1 state is localized in the three-ring subsystem, the S_2 state is mainly confined to the two-ring subsystem. In contrast, for *o*-PPE the S_2 state is delocalized over the entire molecule and we do not find a large contribution from a particular region in the molecule. These results are in agreement with the expected breaking of conjugation when a meta-break is found. This phenomenon was also observed in the study of a similar molecule (two-, three-, and four-ring linear polyphenylene ethynylene units linked by meta-substitutions) where the different excited states were localized in the different linear PPE units.[63]

The time-trace of the length of each ethynylene bond (labeled as in Figure 1), averaged over the 1000 trajectories performed on S_0, S_1, and S_2 for *m*-PPE, is shown in Figure 4. The three ethynylene bonds present similar behavior on the S_0 state, oscillating with a mean of ∼1.203 Å. When excited to the S_1 state, the two triple bonds of the three ring subsystem oscillate with a large amplitude around an average of ∼1.220 Å. The triple bond located in the two-ring unit is basically unchanged from S_0 to S_1. In contrast, when excited from S_0 to S_2 the triple bonds in the three-ring system are unchanged, and the large fluctuation is now seen in the triple bond in the two-ring unit.

These results directly follow from the spatial localization of the electronic transition density, i.e., the excited state is mainly localized either in the three ring subsystem for S_1 or the two-ring subsystem for S_2. The increase in the length of these triple bond distances is a direct effect of that localization.

dx.doi.org/10.1021/jp4102652 | J. Phys. Chem. C 2013, 117, 26517−26528

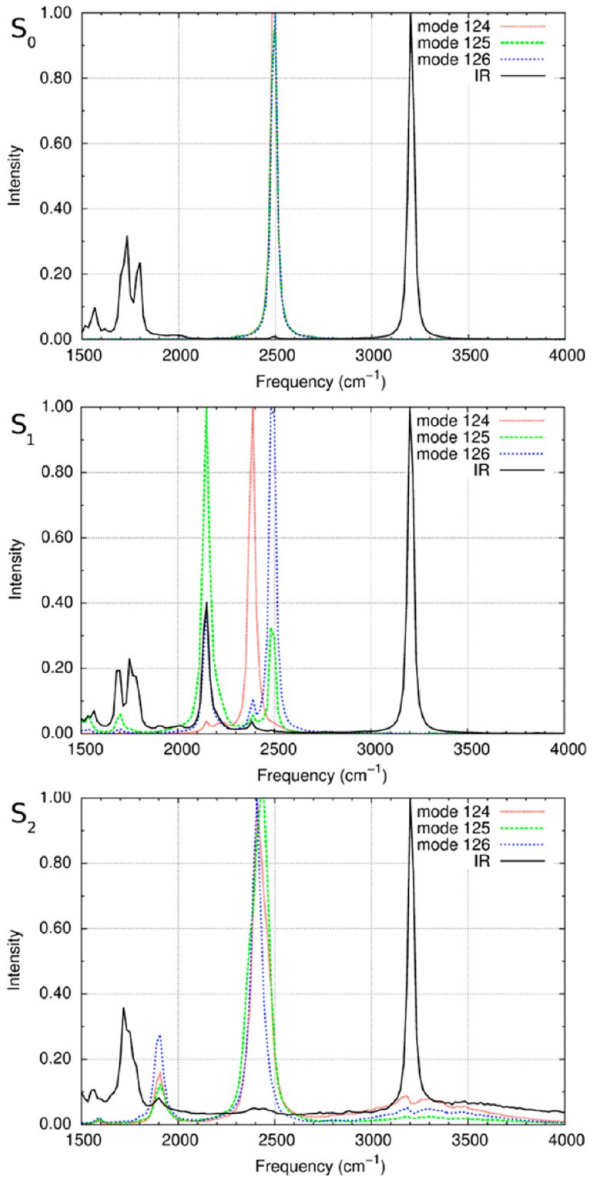

Figure 8. Normal mode displacement spectra. The projection of the ground state normal modes involved in the triple bonds is presented for the first two excited states *m*-PPE.

We analyze now the behavior of the ethynylene bond length in the *o*-PPE molecule (Figure 5). The triple bond distances for the ground state were similar to those of *m*-PPE. This confirms the similarity between the vibrations associated to the C≡C bonds for both molecules in the ground state ESMD simulations and is in agreement with the experimental spectra, since the IR bands associated to C≡C stretching are similar in these systems.[60] The length of all the triple bonds of *o*-PPE during ESMD on S_1 and S_2 is, on average, larger than the values obtained during MD on S_0, showing that the vibrational energy is delocalized throughout the whole molecule. However, not all the ethynylene bonds are equally excited on both excited state surfaces. The ESMD on S_1 reveals a higher excitation of the internal triple bond of the three-ring unit with respect to the others, while a different distribution of the excitation is observed in the ESMD on S_2, where both the triple bond of the two-ring PPE unit as well as the external triple bond of the three-ring unit become lengthened. This effect also arises naturally from the delocalization of the transition density for *o*-PPE.

The assignment of the peaks on the IR spectra to vibrations involving stretching motions of the different acetylene bonds can be obtained by performing a Fourier transform of the time-dependence of the triple bond length displayed in Figure 4. The vibration around 2500 cm^{-1} is IR inactive and is approximately the same for all the triple bonds in the ground state of *m*-PPE (Figure 6). For S_1, the band around 2150 cm^{-1} is shown to be a combination of the triple bond distance oscillations that are located in the three-ring subsystem. These two acetylene distances also give rise to another band at 2400 cm^{-1} that is red-shifted compared to the C≡C bands in the S_0 state. The triple bond located in the two-ring subsystem presents a band that was not changed when moving from the ground state to the S_1 state (2500 cm^{-1}). In the S_2 state, there is a redshift of 100 cm^{-1} for all the triple bond bands with respect to the values obtained during the MD simulation in S_0 (2500 cm^{-1}); however, there is no significant difference between all the bands in the alkyne region (2000 − 2500 cm^{-1}), such as observed for the first excited state. The two-ring acetylene bond presents several peaks between 1000 cm^{-1} and 2000 cm^{-1}, but most of these bands have a small intensity in the IR spectra, hindering their assignment and posterior use as a fingerprint. For both S_0 and S_2, it seems that the C≡C bands are almost inactive in the IR in contrast to the case of S_1. The same analysis was carried out for *o*-PPE (Figure S1).

The analysis of bond-length oscillations is a good approximation to describe the behavior of well localized normal modes, with the triple bonds potentially contributing to more than one normal mode. This is evidenced as several peaks in the FFT of each ethynylene bond.[56] In order to analyze the contribution of each triple bond stretch to the different ground state normal modes of the molecule, we have calculated the participation number[64] of the projection of a unitary vector $\vec{V}_x$ in the direction of each triple bond stretch on the basis of the normal modes, i.e.,

$$\mathcal{P}_x = \left(\sum_j^{3n} (\vec{V}_x \cdot \vec{L}_j)^4\right)^{-1} \tag{28}$$

where the subscript x refers to the different triple bonds in the molecule.

The results are given in Table 1. Values of $\mathcal{P}_x \approx 3n - 6$ correspond to an extreme delocalization of the stretching with an equal contribution among all the normal modes, while values of $\mathcal{P}_x \approx 1$ indicates that the ethynylene bond perfectly matches with a unique normal mode and remarks the absence of any concerted motion involving the mixture of the corresponding triple bond stretch with other nuclear vibrations. The resulting values of $\mathcal{P}_x$ for all the triple bond stretches vary between 2 and 3. That is, the triple bond stretches are delocalized among only two or three modes. The modes presenting the major contributions to the three triple bond stretches are the 124th (2490 cm^{-1}), 125th (2492 cm^{-1}), and 126th (2493 cm^{-1}). For instance, the 126th normal mode is mostly located in the two-ring bond for *m*-PPE, while the 124th and 125th appear to be distributed over the three-ring int. bond and three-ring ext. bond.

Figure 7 presents the normal modes for *m*-PPE and *o*-PPE. The 124th and 125th *m*-PPE S_0 vibrational modes are the C≡C symmetric and the anti-symmetric vibration of the triple bonds located in the three-ring subunit, respectively. The 126th vibration is mainly a symmetric vibration between the two-ring C≡C bond and the three-ring int. C≡C bond.

dx.doi.org/10.1021/jp4102652 | J. Phys. Chem. C 2013, 117, 26517−26528

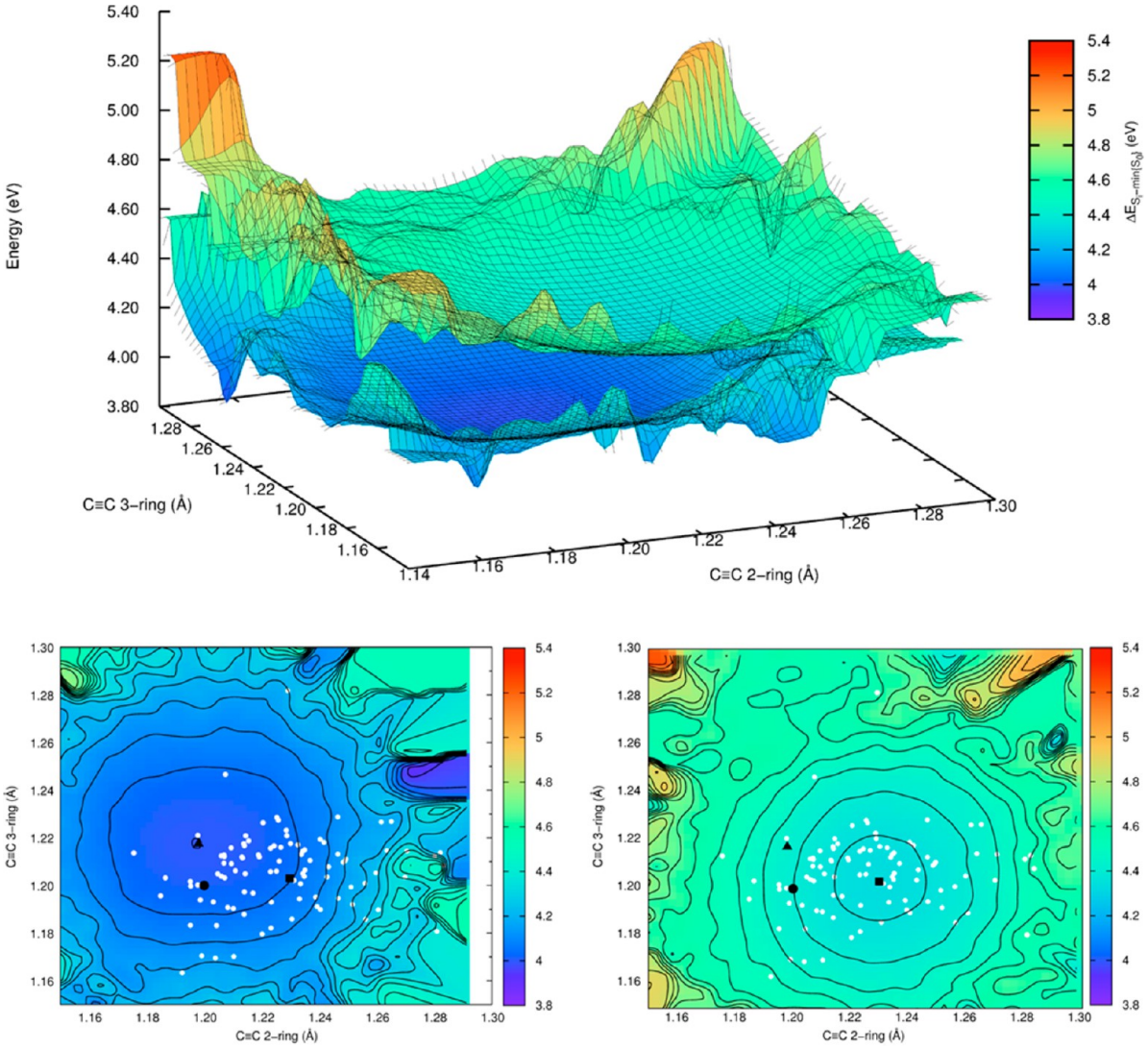

Figure 9. Average potential energy surfaces as a function of two triple bond distances for the S_1 and S_2 excited states. The bottom left surface corresponds to the S_1 state and the right one corresponds to the S_2 state. The white dots correspond to the triple bond distances at which the jump between the S_2 and S_1 states occurs over the 100 different Tully dynamics. The black circle corresponds to the minimum of the S_0 surface, the black triangle is the minimum of the S_1 surface and the black square is the minimum of the S_2 surface.

The FFT of the evolution in time of $Q_{124}(t)$, $Q_{125}(t)$, and $Q_{126}(t)$ on the S_0, S_1, and S_2 states, evaluated from the evolution in terms of Cartesian coordinates according to eq 26, is shown in Figure 8. The three modes, evaluated on the S_0 state, present a common and unique peak at ∼2500 cm^{-1} (Figure 8). This observation is consistent with the common peak, also at ∼2500 cm^{-1}, observed in the FFT of the time dependence of the ethynylene bond lengths shown in Figure 6. One important characteristic of these modes is that only one peak is present in all cases, allowing us to conclude that these modes are not significantly coupled to other modes during the dynamics on S_0 and, therefore, their identities are preserved over time.

The situation becomes more complex for the ESMD simulations, where these modes mix with each other and also with other modes. The analysis of the normal mode motions on the S_1 state of *m*-PPE reveals a strong mixture of the $Q_{125}(t)$ and $Q_{126}(t)$ normal modes, giving rise to two bands (Figure 8). The $Q_{125}(t)$ mode mainly contributes to the intense band located at 2150 cm^{-1}, while the $Q_{126}(t)$ mode is the most important in the band located at 2500 cm^{-1}. Although the latter is common to all ESMD and ground state dynamics, the former is only observed for IR in the S_1 state. On the other hand, a weak coupling of the $Q_{124}(t)$ mode with other modes is evidenced as a shift of the band to 2400 cm^{-1}. In the S_2 state, there is a broad band at 2400 cm^{-1}, which has contributions from the three modes, and a smaller band at 1900 cm^{-1}. This makes the situation similar to the one of S_0, where the spectral distinction between the different normal modes is not possible.

So far, we have shown that in *m*-PPE there are differences in the spatial localization of the electronic transition density on S_1 and S_2: the transition density of S_1 is localized in the three-ring PPE unit, making the band at 2150 cm^{-1} IR active due to changes in the dipole moment of the molecule. The prediction of this band suggests the potential identification of the S_1 state using ultrafast transient IR spectroscopy.

To show the intramolecular vibrational redistribution (IVR), we created free energy surface plots as a function of the triple bond distances (the one from the two ring PPE unit and one from the three ring PPE unit; as both three-ring int. and three-ring ext. produce the same result) using the ESMD snapshots

dx.doi.org/10.1021/jp4102652 | J. Phys. Chem. C 2013, 117, 26517−26528

(Figure 9). These adiabatic potential energy surfaces are obtained as an average over all the ethynylene bond length and electronic excited state energies collected during the ESMD simulations, which effectively makes them free energy surfaces. The S_2 minimum energy well is located at the triple bond lengths of 1.23 Å and 1.20 Å for the two-ring and three-ring *m*-PPE units, respectively, while the S_1 well is the opposite situation, i.e., 1.20 Å and 1.22 Å. For the case of S_0 the well is located at 1.20 Å and 1.20 Å, respectively. In order to analyze the energy transfer processes that take place through S_1-S_2 conical intersections, 100 non-adiabatic excited state molecular dynamics (NAESMD) simulations were performed and the triple bond distances at which the system goes from S_2 to S_1 were plotted on the contour surface energy plots. It is possible to observe that the hops take place close to the minimum of the S_2 surface. Therefore, the minimum of the S_2 potential surface corresponds to a region of strong non-adiabatic coupling with the S_1 state. After the vertical excitation, the system evolves in the S_2 surface, i.e., two-ring subsystem, until it reaches the minimum. At this point, a $S_2 \rightarrow S_1$ hop takes place, with the S_1 state characterized by its localization in the three-ring subsystem, where the system remains until the photon emission is observed from S_1 to S_0. All the process could be monitored using IR spectroscopy, where the characteristic peak at 2150 cm^{-1} can be used as a signal that the S_1 state is populated.

CONCLUSIONS

Several differences have been found between the *o*- and *m*-PPE excited states, especially the localization of the excitation. The meta substituted system seems to differentiate regions in the molecule that are correlated to each excited state, the three-ring system being associated with the S_1 state while the two-ring subsystem is associated with the S_2 state. This phenomenon can be attributed to the break in the π-conjugation of this molecule, and is of great importance to guarantee unidirectional energy transfer in potential applications.

On the basis of the IR results that we obtained and the analysis of the transition density matrices, for *m*-PPE, it is possible to affirm that the phenomenon observed is directly related to the C≡C distances, and that the presence of the sharp peak at 2150 cm^{-1} in the S_1 spectrum is due to a change in the frequency of the normal mode associated with these bonds. Therefore the IVR appears to play an important role in the hop process between the S_2 and S_1 state for *m*-PPE, where the coupling between the antisymmetric and the symmetric S_0 bands gives rise to a new band around 2150 cm^{-1} which is IR active. The importance of identifying the S_1 state resides in the fact that it will be the last excited state reached in an energy transfer process. A particular characterization of this state is crucial for *m*-PPE, since this type of molecule appears to be the best candidate to act as a building block in the design of energy transfer molecules.[9,20]

ASSOCIATED CONTENT

Supporting Information

Figure S1 shows the distance spectra for the triple bond compared to the IR spectra of *o*-PPE. Figure S2 depicts the normal mode displacement spectra for *o*-PPE. This material is available free of charge via the Internet at http://pubs.acs.org.

AUTHOR INFORMATION

Corresponding Author

*Phone: (352) 392-6972. Fax (352) 392-8722. E-mail: roitberg@ufl.edu.

Notes

The authors declare no competing financial interest.

ACKNOWLEDGMENTS

We thank to Natali Di Russo and Dr. Billy Miller III for their comments and suggestion during the writing part of the paper. This work was partially supported by CONICET, UNQ, NSF Grants CHE-0239120 and CHE-0808910. We also want to acknowledge the University of Florida Research Computing for providing computational resources and support that have contributed to the research results reported in this publication.

REFERENCES

(1) Balzani, V.; Credi, A.; Venturi, M. *Molecular Devices and Machines*, 2nd ed.; Wiley-VCH: Weinheim, Germany, 2008.

(2) Varnavski, O.; Leanov, A.; Liu, L.; Takacs, J.; Goodson, T. Large Nonlinear Refraction and Higher Order Nonlinear Optical Effects in a Novel Organic Dendrimer. *J. Phys. Chem. B* **2000**, *104*, 179−188.

(3) Naylor, A. M.; Goddard, W. A.; Kiefer, G. E.; Tomalia, D. A. Starburst Dendrimers. 5. Molecular Shape Control. *J. Am. Chem. Soc.* **1989**, *111*, 2339−2341.

(4) Adronov, A.; Fréchet, J. M. J. Light-harvesting Dendrimers. *Chem. Commun.* **2000**, 1701−1710.

(5) Adronov, A.; Robello, D. R.; Fréchet, J. M. J. Light Harvesting and Energy Transfer Within Coumarin-labeled Polymers. *J. Polym. Sci., Part A: Polym. Chem.* **2001**, *39*, 1366−1373.

(6) Frechet, J. M. Functional Polymers and Dendrimers: Reactivity, Molecular Architecture, and Interfacial Energy. *Science* **1994**, *263*, 1710−1715.

(7) Gilat, S. L.; Adronov, A.; Fréchet, J. M. J. Light Harvesting and Energy Transfer in Novel Convergently Constructed Dendrimers. *Angew. Chem., Int. Ed.* **1999**, *38*, 1422−1427.

(8) Balzani, V.; Ceroni, P.; Juris, A.; Venturi, M.; Campagna, S.; Puntoriero, F.; Serroni, S. Dendrimers Based on Photoactive Metal Complexes. Recent Advances. *Coord. Chem. Rev.* **2001**, *219−221*, 545−572.

(9) Kopelman, R.; Shortreed, M.; Shi, Z.-Y.; Tan, W.; Xu, Z.; Moore, J. S.; Bar-Haim, A.; Klafter, J. Spectroscopic Evidence for Excitonic Localization in Fractal Antenna Supermolecules. *Phys. Rev. Lett.* **1997**, *78*, 1239−1242.

(10) Xu, Z.; Moore, J. S. Design and Synthesis of a Convergent and Directional Molecular Antenna. *Acta Polym.* **1994**, *45*, 83−87.

(11) Shortreed, M. R.; Swallen, S. F.; Shi, Z.-Y.; Tan, W.; Xu, Z.; Devadoss, C.; Moore, J. S.; Kopelman, R. Directed Energy Transfer Funnels in Dendrimeric Antenna Supermolecules. *J. Phys. Chem. B* **1997**, *101*, 6318−6322.

(12) Ortiz, W.; Krueger, B. P.; Kleiman, V. D.; Krause, J. L.; Roitberg, A. E. Energy Transfer in the Nanostar: The Role of Coulombic Coupling and Dynamics. *J. Phys. Chem. B* **2005**, *109*, 11512−11519.

(13) Palma, J. L.; Atas, E.; Hardison, L.; Marder, T. B.; Collings, J. C.; Beeby, A.; Melinger, J. S.; Krause, J. L.; Kleiman, V. D.; Roitberg, A. E. Electronic Spectra of the Nanostar Dendrimer: Theory and Experiment†. *J. Phys. Chem. C* **2010**, *114*, 20702−20712.

(14) Melinger, J. S.; Pan, Y.; Kleiman, V. D.; Peng, Z.; Davis, B. L.; McMorrow, D.; Lu, M. Optical and Photophysical Properties of Light-Harvesting Phenylacetylene Monodendrons Based on Unsymmetrical Branching. *J. Am. Chem. Soc.* **2002**, *124*, 12002−12012.

(15) Kleiman, V. D.; Melinger, J. S.; McMorrow, D. Ultrafast Dynamics of Electronic Excitations in a Light-Harvesting Phenylacetylene Dendrimer. *J. Phys. Chem. B* **2001**, *105*, 5595−5598.

(16) Kuroda, D. G.; Singh, C. P.; Peng, Z.; Kleiman, V. D. Mapping Excited-State Dynamics by Coherent Control of a Dendrimer's Photoemission Efficiency. *Science* **2009**, *326*, 263−267.

(17) Wu, C.; Malinin, S. V.; Tretiak, S.; Chernyak, V. Y. Exciton Scattering and Localization in Branched Dendrimeric Structures. *Nat. Phys.* **2006**, *2*, 631−635.

(18) Pan, Y.; Lu, M.; Peng, Z.; Melinger, J. S. Synthesis and Optical Properties of Unsymmetrical Conjugated Dendrimers Focally Anchored

with Perylenes in Different Geometries. *J. Org. Chem.* **2003**, *68*, 6952−6958.
(19) Fernandez-Alberti, S.; Roitberg, A. E.; Kleiman, V. D.; Nelson, T.; Tretiak, S. Shishiodoshi Unidirectional Energy Transfer Mechanism in Phenylene Ethynylene Dendrimers. *J. Chem. Phys.* **2012**, *137*, 22A526−22A526−9.
(20) Egbe, D. A. M.; Roll, C. P.; Klemm, E. Synthesis, Characterisation and Properties of Highly Luminescent and Liquid-crystalline Alternating PPE/PPV-copolymers. *Des. Monomers Polym.* **2002**, *5*, 245−275.
(21) Goodson, T. Time-resolved Spectroscopy of Organic Dendrimers and Branched Chromophores. In *Annual Review of Physical Chemistry*; Annual Reviews: Palo Alto, CA, 2005; Vol. 56, pp 581−603.
(22) Huang, W. Y.; Gao, W.; Kwei, T. K.; Okamoto, Y. Synthesis and Characterization of Poly(alkyl-substituted P-phenylene Ethynylene)s. *Macromolecules* **2001**, *34*, 1570−1578.
(23) Yin, S.; Leen, V.; Jackers, C.; Van der Auweraer, M.; Smet, M.; Boens, N.; Dehaen, W. The Synthesis and Spectroscopic Characterization of Poly(p-phenylene Ethynylene) with 3-connected BODIPY End Groups. *Dyes Pigments* **2011**, *88*, 372−377.
(24) Fernandez-Alberti, S.; Kleiman, V. D.; Tretiak, S.; Roitberg, A. E. Nonadiabatic Molecular Dynamics Simulations of the Energy Transfer Between Building Blocks in a Phenylene Ethynylene Dendrimer. *J. Phys. Chem. A* **2009**, *113*, 7535−7542.
(25) Kirkwood, J. C.; Scheurer, C.; Chernyak, V.; Mukamel, S. Simulations of Energy Funneling and Time- and Frequency-gated Fluorescence in Dendrimers. *J. Chem. Phys.* **2001**, *114*, 2419−2429.
(26) Tortschanoff, A.; Mukamel, S. Pump−Probe Simulation Study of the Two-Exciton Manifold of Dendrimers. *J. Phys. Chem. A* **2002**, *106*, 7521−7529.
(27) Hardison, L. M.; Zhao, X.; Jiang, H.; Schanze, K. S.; Kleiman, V. D. Energy Transfer Dynamics in a Series of Conjugated Polyelectrolytes with Varying Chain Length. *J. Phys. Chem. C* **2008**, *112*, 16140−16147.
(28) Atas, E.; Peng, Z.; Kleiman, V. D. Energy Transfer in Unsymmetrical Phenylene Ethynylene Dendrimers. *J. Phys. Chem. B* **2005**, *109*, 13553−13560.
(29) Chen, Y.; Palmer, P. M.; Topp, M. R. Infrared Spectroscopy of Jet-cooled, Electronically Excited Clusters of Coumarin 151: Excited-state Interactions and Conformational Relaxation. *Int. J. Mass Spectrom.* **2002**, *220*, 231−251.
(30) Weiler, M.; Bartl, K.; Gerhards, M. Infrared/ultraviolet Quadruple Resonance Spectroscopy to Investigate Structures of Electronically Excited States. *J. Chem. Phys.* **2012**, *136*, 114202−114202−6.
(31) Seurre, N.; Le Barbu-Debus, K.; Lahmani, F.; Zehnacker-Rentien, A.; Sepioł, J. Electronic and Vibrational Spectroscopy of Jet-cooled M-cyanophenol and Its Dimer: Laser-induced Fluorescence and Fluorescence-dip IR Spectra in the S0 and S1 States. *Chem. Phys.* **2003**, *295*, 21−33.
(32) Zhang, Y.; Kubicki, J.; Platz, M. S. Ultrafast UV−Visible and Infrared Spectroscopic Observation of a Singlet Vinylcarbene and the Intramolecular Cyclopropenation Reaction. *J. Am. Chem. Soc.* **2009**, *131*, 13602−13603.
(33) Zhang, Y.; Burdzinski, G.; Kubicki, J.; Vyas, S.; Hadad, C. M.; Sliwa, M.; Poizat, O.; Buntinx, G.; Platz, M. S. Study of the S1 Excited State of para-Methoxy-3-phenyl-3-methyl Diazirine by Ultrafast Time Resolved UV−Vis and IR Spectroscopies and Theory. *J. Am. Chem. Soc.* **2009**, *131*, 13784−13790.
(34) Vyas, S.; Kubicki, J.; Luk, H. L.; Zhang, Y.; Gritsan, N. P.; Hadad, C. M.; Platz, M. S. An Ultrafast Time-resolved Infrared and UV−vis Spectroscopic and Computational Study of the Photochemistry of Acyl Azides. *J. Phys. Org. Chem.* **2012**, *25*, 693−703.
(35) Dougherty, T. P.; Heilweil, E. J. Ultrafast Transient Infrared Absorption Studies of M(CO)6 (M = Cr, Mo or W) Photoproducts in N-hexane Solution. *Chem. Phys. Lett.* **1994**, *227*, 19−25.
(36) Szabo, A. *Modern Quantum Chemistry: Introduction to Advanced Electronic Structure Theory*; Courier Dover Publications: Mineola, NY, 1996.
(37) Jamorski, C.; Casida, M. E.; Salahub, D. R. Dynamic Polarizabilities and Excitation Spectra from a Molecular Implementation of Time-dependent Density-functional Response Theory: N2 as a Case Study. *J. Chem. Phys.* **1996**, *104*, 5134.
(38) Weiner, B.; Trickey, S. B. Time-Dependent Variational Principle in Density Functional Theory. In *Advances in Quantum Chemistry*; Per-Olov Löwdin, Ed.; Academic Press: San Diego, CA, 1999; Vol. 35, pp 217−247.
(39) Weiner, B.; Trickey, S. B. State Energy Functionals and Variational Equations in Density Functional Theory. *J. Mol. Struct. THEOCHEM* **2000**, *501−502*, 65−83.
(40) Tretiak, S.; Mukamel, S. Density Matrix Analysis and Simulation of Electronic Excitations in Conjugated and Aggregated Molecules. *Chem. Rev.* **2002**, *102*, 3171−3212.
(41) Cook, D. B. *Handbook Of Computational Quantum Chemistry*; Dover Publications, Incorporated: Mineola, NY, 2005.
(42) Nelson, T.; Fernandez-Alberti, S.; Chernyak, V.; Roitberg, A. E.; Tretiak, S. Nonadiabatic Excited-State Molecular Dynamics Modeling of Photoinduced Dynamics in Conjugated Molecules. *J. Phys. Chem. B* **2011**, *115*, 5402−5414.
(43) Dewar, M. J. S.; Zoebisch, E. G.; Healy, E. F.; Stewart, J. J. P. Development and Use of Quantum Mechanical Molecular Models. 76. AM1: a New General Purpose Quantum Mechanical Molecular Model. *J. Am. Chem. Soc.* **1985**, *107*, 3902−3909.
(44) Tretiak, S.; Chernyak, V. Resonant Nonlinear Polarizabilities in the Time-dependent Density Functional Theory. *J. Chem. Phys.* **2003**, *119*, 8809−8823.
(45) Tully, J. C. Molecular Dynamics with Electronic Transitions. *J. Chem. Phys.* **1990**, *93*, 1061−1071.
(46) Hammes-Schiffer, S.; Tully, J. C. Proton Transfer in Solution: Molecular Dynamics with Quantum Transitions. *J. Chem. Phys.* **1994**, *101*, 4657−4667.
(47) Gordon, R. G. Correlation Functions for Molecular Motion. *Adv. Magn. Reson.* **1968**, *3*, 1−42.
(48) Kalstein, A.; Fernández-Alberti, S.; Bastida, A.; Soler, M. A.; Farag, M. H.; Zúñiga, J.; Requena, A. Vibrational Dynamics of Polyatomic Molecules in Solution: Assignment, Time Evolution and Mixing of Instantaneous Normal Modes. *Theor. Chem. Acc.* **2011**, *128*, 769−782.
(49) Ferrer, F. J. A.; Santoro, F. Comparison of Vertical and Adiabatic Harmonic Approaches for the Calculation of the Vibrational Structure of Electronic Spectra. *Phys. Chem. Chem. Phys.* **2012**, *14*, 13549−13563.
(50) Callen, H. B.; Welton, T. A. Irreversibility and Generalized Noise. *Phys. Rev.* **1951**, *83*, 34−40.
(51) Schatz, G. C.; Ratner, M. A. *Quantum Mechanics in Chemistry*, 1st ed.; Dover Publications: Mineola, NY, 2002.
(52) Jeon, J.; Yang, S.; Choi, J.; Cho, M. Computational Vibrational Spectroscopy of Peptides and Proteins in One and Two Dimensions. *Acc. Chem. Res.* **2009**, *42*, 1280−1289.
(53) Gaigeot, M. P.; Sprik, M. Ab Initio Molecular Dynamics Computation of the Infrared Spectrum of Aqueous Uracil. *J. Phys. Chem. B* **2003**, *107*, 10344−10358.
(54) Gaigeot, M. P.; Vuilleumier, R.; Sprik, M.; Borgis, D. Infrared Spectroscopy of N-Methylacetamide Revisited by Ab Initio Molecular Dynamics Simulations. *J. Chem. Theory Comput.* **2005**, *1*, 772−789.
(55) Tannor, D. J. *Introduction to Quantum Mechanics: A Time-Dependent Perspective*; University Science Books: Sausalito, CA, 2006.
(56) Stendardo, E.; Avila Ferrer, F.; Santoro, F.; Improta, R. Vibrationally Resolved Absorption and Emission Spectra of Dithiophene in the Gas Phase and in Solution by First-Principle Quantum Mechanical Calculations. *J. Chem. Theory Comput.* **2012**, *8*, 4483−4493.
(57) Frisch, M. J.; Trucks, G. W.; Schlegel, H. B.; Scuseria, G. E.; Robb, M. A.; Cheeseman, J. R.; Scalmani, G.; Barone, V.; Mennucci, B.; Petersson, G. A.; et al. *Gaussian 09*, revision A.1; Gaussian Inc.: Wallingford CT, 2009.
(58) Wang, J.; Wolf, R. M.; Caldwell, J. W.; Kollman, P. A.; Case, D. A. Development and Testing of a General Amber Force Field. *J. Comput. Chem.* **2004**, *25*, 1157−1174.
(59) Case, D. A.; Darden, T. A.; Cheatham III, T. E.; Simmerling, C. L.; Wang, J.; Duke, R. E.; Luo, R.; Walker, R. C.; Zhang, W.; Merz, K. M.; et al. *AMBER 12*; University of California, San Francisco, 2012.

(60) Trumbo, D. L.; Marvel, C. S. Polymerization Using Palladium (II) Salts: Homopolymers and Copolymers from Phenylethynyl Compounds and Aromatic Bromides. *J. Polym. Sci., Part A: Polym. Chem.* **1986**, *24*, 2311−2326.
(61) Gaigeot, M.-P. Theoretical Spectroscopy of Floppy Peptides at Room Temperature. A DFTMD Perspective: Gas and Aqueous Phase. *Phys. Chem. Chem. Phys.* **2010**, *12*, 3336−3359.
(62) Tretiak, S.; Isborn, C. M.; Niklasson, A. M. N.; Challacombe, M. Representation Independent Algorithms for Molecular Response Calculations in Time-dependent Self-consistent Field Theories. *J. Chem. Phys.* **2009**, *130*, 054111−054111−16.
(63) Fernandez-Alberti, S.; Kleiman, V. D.; Tretiak, S.; Roitberg, A. E. Unidirectional Energy Transfer in Conjugated Molecules: The Crucial Role of High-Frequency C≡C Bonds. *J. Phys. Chem. Lett.* **2010**, *1*, 2699−2704.
(64) Bell, R. J.; Dean, P.; Hibbins-Butler, D. C. Localization of Normal Modes in Vitreous Silica, Germania and Beryllium Fluoride. *J. Phys. C Solid State Phys.* **1970**, *3*, 2111.